J. Fluid Mech. (1997), *vol.* 351, *pp.* 17–39. Printed in the United Kingdom

© 1997 Cambridge University Press

Statistical sand wave dynamics in one-directional water flows

By VLADIMIR I. NIKORA[1], ALEXANDER N. SUKHODOLOV[2] AND PAWEL M. ROWINSKI[3]

[1] National Institute of Water and Atmospheric Research, Christchurch, PO Box 8602, New Zealand

[2] Institute of Geophysics and Geology, Moldova's Academy of Sciences, 3 Academiei street, 277028 Kishinev, Republic of Moldova

[3] Institute of Geophysics, Polish Academy of Sciences, ul. Ksiecia Janusza 64, 01-452 Warszawa, Poland

(Received 4 January 1996 and in revised form 20 May 1997)

Moving sand waves and the overlying tubulent flow were measured on the Wilga River in Poland, and the Tirnava Mica and Buzau Rivers in Romania. Bottom elevations and flow velocities were measured at six points simultaneously by multi-channel measuring systems. From these data, the linear and two-dimensional sections of the three-dimensional correlation and structure functions and various projections of sand wave three-dimensional spectra were investigated.

It was found that the longitudinal wavenumber spectra of the sand waves in the region of large wavenumbers followed Hino's -3 law ($S(K_x) \propto K_x^{-3}$) quite satisfactorily, confirming the theoretical predictions of Hino (1968) and Jain & Kennedy (1974). However, in contrast to Hino (1968), the sand wave frequency spectrum in the high-frequency region was approximated by a power function with the exponent -2, while in the lower-frequency region this exponent is close to -3.

A dispersion relation for sand waves has been investigated from analysis of structure functions, frequency spectra and the cross-correlation functions method. For wavelengths less than 0.15–0.25 of the flow depth, their propagation velocity C is inversely proportional to the wavelength λ. When the wavelengths of spectral components are as large as 3–4 times the flow depth, no dispersion occurs. These results proved to be in good qualitative agreement with the theoretical dispersion relation derived from the potential-flow-based analytical models (Kennedy 1969; Jain & Kennedy 1974). We also present another, physically-based, explanation of this phenomenon, introducing two types of sand movement in the form of sand waves. The first type (I) is for the region of large wavenumbers (small wavelengths) and the second one (II) is for the region of small wavenumbers (large wavelengths). The small sand waves move due to the motion of individual sand particles (type I, $C \propto \lambda^{-1}$) while larger sand waves propagate as a result of the motion of smaller waves on their upstream slopes (type II, $C \propto \lambda^{0}$). Like the sand particles in the first type, these smaller waves redistribute sand from upstream slopes to downstream ones. Both types result in sand wave movement downstream but with a different propagation velocity.

The main characteristics of turbulence, as well as the quantitative values characterizing the modulation of turbulence by sand waves, are also presented.

https://doi.org/10.1017/S0022112097006708 Published online by Cambridge University Press

1. Introduction

The movement of sand waves in one-directional water flows (rivers, canals, seabed currents, etc.) is a complicated natural phenomenon determining the bottom sediment transport and hydraulic resistance. Despite the intensive survey of sand wave morphometry and dynamics and progress in understanding these phenomena, some problems remain unsolved. One of them concerns the sand wave statistical dynamics expressed in frequency and wavenumber spectra, as well as other characteristics that describe their space–time structure. Most of the works on the statistical dynamics of sand waves are based upon the analysis of bottom longitudinal profiles obtained in laboratory experiments (Nordin & Algert 1966; Fukuoka 1968; Jain & Kennedy 1974; Shen & Cheong 1977; Engel & Lau 1980; Tsujimoto & Nakagawa 1983; Nikora 1987) and in the field (Nordin 1971; Annambhotla, Sayre & Livesey 1972; Levey, Kjerfve & Getzen 1980; Baliga & Hudspeth 1981; Nikora 1983). Only a few of these works were devoted to investigations of temporal profiles of bottom elevation. The authors are familiar with only one investigation of bottom wave frequency properties in field conditions (Dinehart 1989), but the scaling in the frequency spectra and dispersion relationship were not investigated in that work.

1.1. *Wavenumber spectrum*

The most substantial result of the above-mentioned works was the discovery and confirmation of the scaling region in the longitudinal wavenumber spectrum (Hino 1968; Jain & Kennedy 1974)

$$S(K_x) = A_x K_x^{-3}, \quad K_{x0} < K_x, \tag{1}$$

where $S(K_x)$ is the wavenumber spectrum of bed elevations in the main flow direction, K_x is the longitudinal wavenumber ($K_x = 2\pi/\lambda$, λ is the wavelength), K_{x0} is the wavenumber that restricts applicability of (1), and A_x is some non-dimensional parameter. The parameter A_x was initially regarded as a universal constant (Hino 1968), but subequent analysis of data in respect to ripples and dunes in different rivers (Nikora 1983) showed its almost square connection with Froude number ($A_x \propto Fr^{2.1}$, $Fr = u/(gh)^{1/2}$, where u is the vertically averaged flow velocity, g is the gravitational acceleration, and h is the flow depth). Besides, it was established that the spectral -3 law is valid not only for small scales, that correspond to ripples and dunes, but also for scales commensurable with the river width (Grinvald & Nikora 1988). The empirical wavenumber spectra of bottom longitudinal profiles that were obtained by Nikora, Borik & Kuzmin (1988) and Grinvald & Nikora (1988) are characterized by several scaling regions with $S(K_x) = A_{xi} K_x^{-3}$. A sketch of this spectrum is shown in figure 1. The scaling regions are divided by spectral maxima corresponding to river bedforms with scales varying from those of the flow depth to several tens of river width. The behaviour of spectra in scaling regions is described by the common relationship

$$S(K_x) = A_{xi} K_x^{-3}, \tag{2}$$

where A_{xi} is interpreted as the square of the characteristic steepness of bedforms that make up the ith scaling region in the spectrum (Nikora 1983; Grinvald & Nikora 1988). The A_{xi} value increases from small wavenumber scaling regions to the large ones (figure 1). For instance, for the Dniester River (Ukraine) A_{xi} changes from 10^{-5} on scales of about 1 km (7 river widths) to 10^{-3} on scales of the flow depth. (Here we present the estimates obtained for spectra, the whole energy of which is concentrated in the positive region of wavenumbers and angular frequencies. Unlike Hino (1968) we

https://doi.org/10.1017/S0022112097006708 Published online by Cambridge University Press

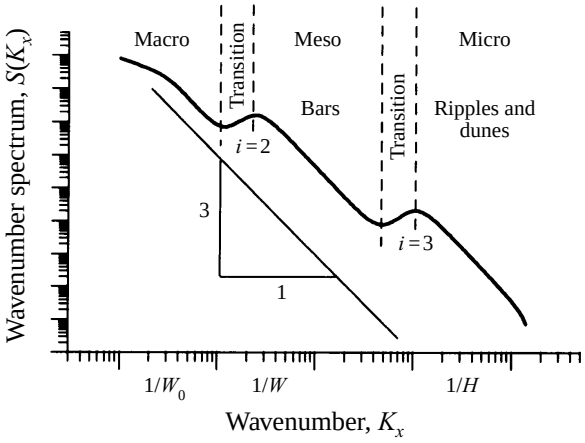


FIGURE 1. Schematic spectrum of the longitudinal profile of bed elevations in sand rivers showing three scaling regions: macro, meso, and micro, characterized by three length scales; flow depth H, river width W, and valley width W_0.

consider not the two-sided spectra with circular frequencies but the single-sided spectra with angular frequencies.) The right-side scaling region in the spectrum $S(K_x)$, which we are going to consider in this paper, corresponds to ripples and dunes (figure 1). It is also noteworthy that Hino's (1968) spectral -3 law reflects the spatial self-similarity of sand wave longitudinal profiles that follows from the relationship $S(K_x) \propto K_x^{-(2H+1)}$ (Mandelbrot 1982). Hurst's exponent H is equal to 1 for the self-similarity situation, while for self-affinity H is less than 1.

In a few studies, the exponent in relationship (1) is not considered as universal. Shen & Cheong (1977), for example, concluded from laboratory and field data that the exponent changes from -4 on ripply bottoms to -3 with fully developed dunes.

1.2. *Frequency spectrum and dispersion relation*

Sand wave frequency spectra have been investigated less comprehensively, and the scaling relationships

$$S(\omega) \propto \omega^{-2}, \quad \omega_0 < \omega < \omega_1, \tag{3}$$

$$S(\omega) \propto \omega^{-3}, \quad \omega_1 < \omega < \omega_\infty \tag{4}$$

proposed by Hino (1968) have been explored only from limited laboratory experiments (Ashida & Tanaka 1967; Nikora 1987). The following dispersion relations correspond to formulae (1), (3) and (4):

$$C(K_x) \propto K_x \quad \text{or} \quad \omega \propto K_x^2, \quad \omega_0 < \omega < \omega_1, \tag{5}$$

$$C(K_x) \propto K_x^0 \quad \text{or} \quad \omega \propto K_x, \quad \omega_1 < \omega < \omega_\infty, \tag{6}$$

where C is the analogue of phase velocity for sand waves, ω is the angular frequency ($\omega = 2\pi/T$), ω_0 and ω_1 are the frequencies restricting scaling regions (3) and (4).

Shen & Cheong (1977) suggested a more general formulae for the dispersion relation

$$C(K_x) \propto K_x^\theta \quad \text{or} \quad \omega \propto K_x^{\theta+1}, \quad \theta > 0, \tag{7}$$

and for the sand wave frequency spectrum

$$S(\omega) \propto \omega^{-\xi}, \tag{8}$$

where $\xi = (\beta+\theta)/(\theta+1)$, θ is the positive exponent, and β is the scaling exponent in

https://doi.org/10.1017/S0022112097006708 Published online by Cambridge University Press

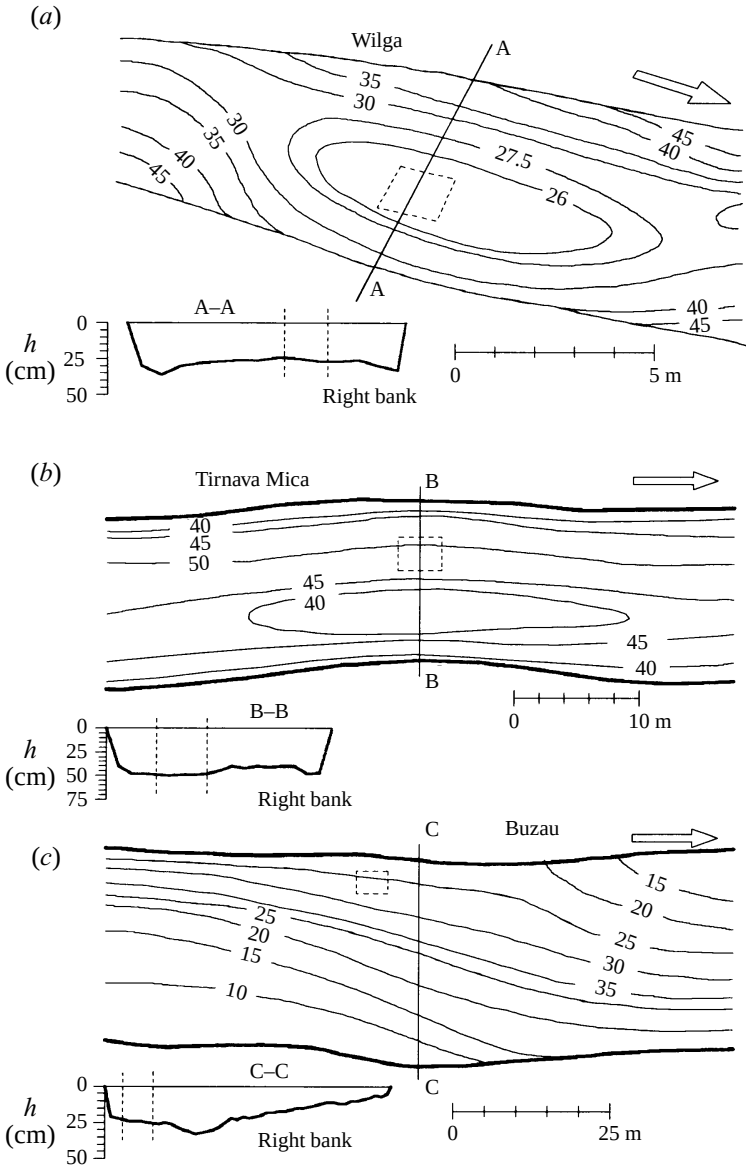


FIGURE 2. Plan views and cross-sections of experimental river reaches; (*a*) Wilga, Poland; (*b*) Tirnava Mica, Romania; and (*c*) Buzau, Romania (dashed boxes show the places where radiators were located).

the wavenumber spectrum. When $\theta = 1$, relationship (7) corresponds to dispersion relationship (5) (also obtained theoretically by Jain & Kennedy (1974) for sand waves in the region of large wavenumbers). In the work of Shen & Cheong (1977), the empirical frequency spectra of sand waves in the flume are also given. In contrast to Hino's (1968) results, they are close to relationship (3) in the high-frequency region and to relationship (4) in the low-frequency region. It should be also added that Shen & Cheong (1977), Baliga & Hudspeth (1981), Nikora (1983, 1987) and Cheong (1992) regarded sand wave field as non-dispersive and subject to relationship (6).

The above short review highlights some contradictions in the interpretation of sand

https://doi.org/10.1017/S0022112097006708 Published online by Cambridge University Press

Q ($m^3\ s^{-1}$)	H (m)	W (m)	u ($m\ s^{-1}$)	u_* ($cm\ s^{-1}$)	I	Ch $m^{0.5}\ s^{-1}$	Fr	Re ($\times 10^{-5}$)	p ($g\ l^{-1}$)	d (mm)
The Wilga River (Poland)										
0.321–0.574	0.19–0.30	6.91–7.07	0.24–0.28	2.7–3.4	0.000 40	24.0–28.7	0.15–0.18	0.47–0.80	0.010	0.35
The Tirnava Mica River (Romania)										
2.09–3.19	0.33–0.41	17.0–18.0	0.37–0.43	3.3–3.7	0.000 34	34.9–36.4	0.20–0.21	1.2–1.8	0.034	0.64
The Buzau River (Romania)										
2.42–3.55	0.18–0.24	47.0–48.0	0.30–0.32	3.3–3.8	0.000 59–0.000 61	23.1–28.9	0.20–0.24	0.57–0.72	0.024	0.31

TABLE 1. Ranges of hydraulic and morphometric characteristics for the experimental river reaches. Here: Q is the water discharge; H is the averaged (cross-sectionally) depth; W is the river width; u is the averaged (cross-sectionally) velocity; u_* is the friction velocity, $u_* = (gHI)^{1/2}$; I is the water surface slope; Ch is the Chezy parameter, $Ch = U/(HI)^{1/2}$; Fr is the Froude number, $Fr = U/(gH)^{1/2}$; Re is the Reynolds number, $Re = UH/\nu$; p is the water turbidity; and d is the mean diameter of bottom sand.

wave spectral dynamics. Further investigations are necessary for their clarification, and priority should be given to obtaining more field data.

The purpose of this work is to further investigate the space–time structure of sand waves (ripples and dunes) on the basis of synchronous measurements of time fluctuations of bottom elevations at spatially fixed verticals. Also, an attempt has been made to evaluate some properties of the flow turbulence over the surveyed sand waves. The preliminary results of this paper, concerning only the Wilga River (Poland), were reported in Nikora *et al.* (1995).

2. Field measurements

The field measurements were carried out in September 1993 on the Wilga River (Poland) and in September 1994 on the Tirnava Mica River (Romania) and the Buzau River (Romania). Plans and profiles of the experimental sections are shown in figure 2, while table 1 contains the main hydraulic and morphometric characteristics.

The field survey comprised systematic hydrometric measurements (water discharge, water level, water surface slope, bottom configuration, etc.) and special field experiments for studying the dynamics of sand waves and for obtaining the characteristics of the stream turbulence over them.

A six-channel microsounder Sh-1, designed and manufactured at the Institute of Geophysics and Geology of Moldova's Academy of Sciences, was used to measure the bottom elevations. The measuring system consists of six sound radiators, a microsounder and a laptop computer. This system permitted synchronous measurements of bottom elevations at six spatially fixed verticals with any sampling rate lower than 2 Hz. The accuracy of the stream depth measurements within the 6–100 cm range was 1–2 mm. To reduce flow disturbances by the radiators we used a specially designed frame (figure 3) that allowed minimal immersing of the radiators in the water flow (1.0–1.5 cm). The frame with the sound radiators was placed in the zone of the stream with quasi-homogeneous hydraulic conditions, i.e. the spatial variability of the flow depth, vertically averaged velocity and sand wave parameters were reasonably small (the zones are shown as dashed boxes in figure 2). Also, we were lucky to have

https://doi.org/10.1017/S0022112097006708 Published online by Cambridge University Press

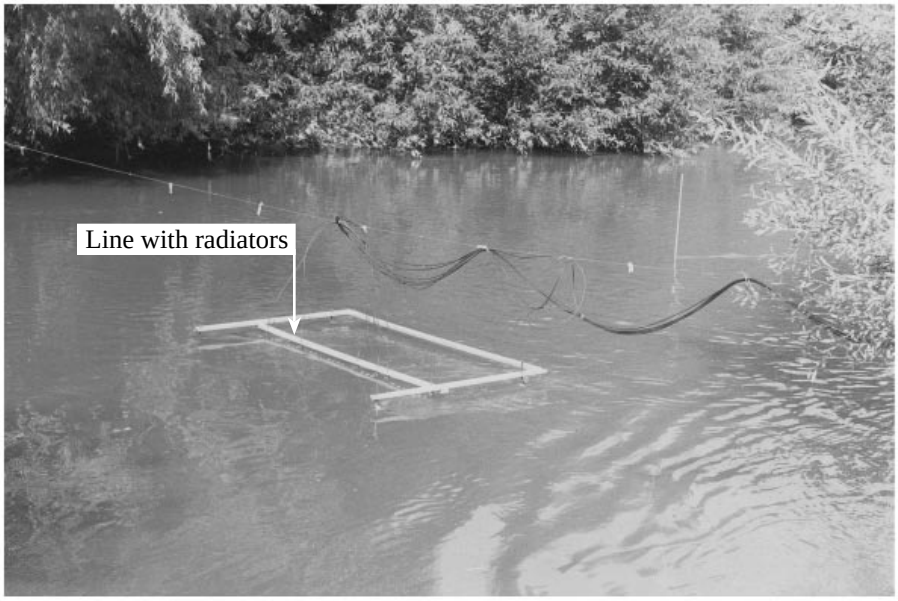


FIGURE 3. Typical setting of the field experiments (The Tirnava Mica River, Romania). The frame with radiators across the flow is shown.

N	Radiator locations	Δt (s)	T (hr)	Δx_{min} (m)	Δx_{max} (m)	u (m s^{-1})	h (m)	u_* (cm s^{-1})
			The Wilga River (Poland)					
1	Longitudinal	15	7.3	0.10	0.70	0.35	0.25	3.1
2	Transversal	15	5.5	0.10	0.70	0.34	0.22	2.9
			The Tirnava Mica River (Romania)					
1	Longitudinal	20	22.6	0.10	1.70	0.48	0.45	3.9
2	Transversal	20	23.5	0.10	1.70	0.48	0.40	3.7
			The Buzau River (Romania)					
1	Longitudinal	15	19.3	0.05	1.15	0.45	0.26	3.9
2	Transversal	4	17.5	0.05	1.15	0.45	0.26	3.9

TABLE 2. Characteristics of the experiments. Here: Δt is the time sampling interval, T is the period of measurements; Δx_{min} and Δx_{max} are the minimum and maximum distances between radiators; u is the vertically averaged velocity over measured sand waves; h is the time-averaged depth over measured sand waves; and u_* is the friction velocity over measured sand waves, $u_* = (ghI)^{1/2}$.

quasi-steady hydraulic conditions during the measurements: the temporal variability of the water discharge and water level did not exceed 5%. This allowed us to consider the sand wave fields investigated to be stationary and homogeneous. Therefore, we could avoid any preliminary data filtering and could directly apply in our analysis methods of the theory of stationary and homogeneous random fields (Monin & Yaglom 1975; Bendat & Piersol 1980; Grinvald & Nikora 1988).

Two main deployment schemes of the micro-sounder radiators were used during the field experiments: (i) along the flow and (ii) across the flow. The measurements carried out along the flow were aimed at studying the longitudinal structure of sand waves, while those carried out across the flow were intended for studying their transverse structure. The main characteristics of these field experiments are given in table 2. In all

https://doi.org/10.1017/S0022112097006708 Published online by Cambridge University Press

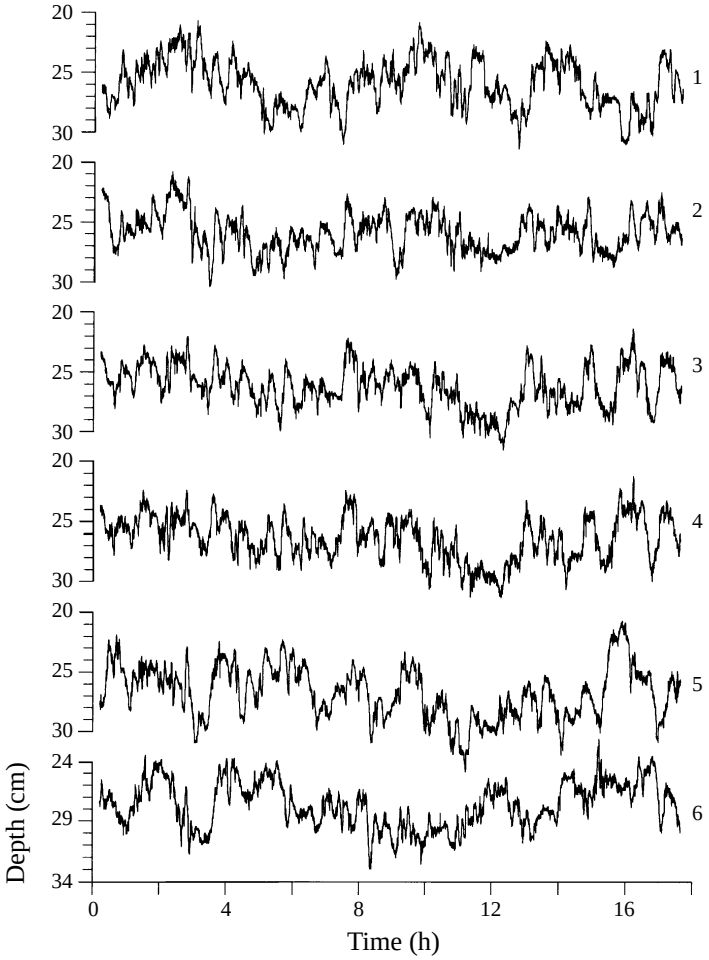


FIGURE 4. Examples of depth (radiator elevation minus bottom elevation) time series for the transverse sounder radiator location, the Buzau River, Romania ($1, 2, \ldots, 6$ denote different measuring verticals; distances between them are: 1–2 = 30 cm; 2–3 = 10 cm; 3–4 = 5 cm; 4–5 = 20 cm; 5–6 = 50 cm, sampling interval 4 s).

cases, bottom elevations were measured at six points simultaneously. Figure 4 shows typical examples of the depth (radiator elevation minus bottom elevation) time series with sampling interval 4 s for the Buzau River.

In several cases we also measured the instantaneous velocities of the flow over the moving sand waves. Micropropeller current meters in a special measuring system (Nikora *et al.* 1994) were used to measure the longitudinal velocities of the flow simultaneously with the measurements of the bottom elevation fluctuations. The main reason for these measurements was to evaluate turbulence characteristics on the surveyed sections. Also, an attempt was made to estimate the degree of modulation of the stream turbulence by the moving sand waves. The details of turbulence measurements will be given in §4.

https://doi.org/10.1017/S0022112097006708 Published online by Cambridge University Press

3. Analysis of sand wave dynamics

Two approaches are used for describing the geometry and dynamics of sand waves (Grinvald & Nikora 1988). With the first, the wavy bottom surface is regarded as a set of visible sand waves, with each separate wave being regarded as a physical object described by a system of geometric (length, height, steepness, etc.) and kinematic (velocity of propagation) parameters. It is this traditional approach that is used in the majority of works devoted to sand waves. According to the second approach the sand waves are regarded as a moving random field of bottom elevations $Z(x, y, t)$ (origin of Z is lower than channel bed surface, at an arbitrary level), where x and y are the longitudinal (the main flow direction) and transversal coordinates, and t is time. A complete picture of such a field is provided by the n-dimensional probability density when $n \to \infty$, which contains full information about the bottom sand wave relief. Quantitative description of sand waves by means of n-dimensional probability functions is theoretically possible, but in practice it entails great difficulties. In this situation an acceptable compromise is the utilization of moment functions (correlations, spectra, structure functions, etc.) for a quantitative evaluation of the sand wave field.

In general, the spectrum of the bottom elevation field $Z(x, y, t)$ is a function of six variables: spatial coordinates x and y, time t, projections K_x and K_y of the wave vector $\boldsymbol{K}$, and the time frequency ω. For the already steady sand waves we can accept the hypothesis of quasi-stationarity and of local spatial homogeneity that reduces their description to the three-dimensional spectrum $S(K_x, K_y, \omega)$, the correlation function $R(\Delta x, \Delta y, \tau)$ and the structure function $D(\Delta x, \Delta y, \tau)$. Functions $S(K_x, K_y, \omega)$, $R(\Delta x, \Delta y, \tau)$ and $D(\Delta x, \Delta y, \tau)$ provide a rather complete description of the sand wave structure and, to a certain degree, are connected with the traditional model of visible sand waves. For instance, the average height h_w of visible sand waves is connected with the root-mean-square deviation of bottom elevations σ_z by means of the relationship $h_w = m\sigma_z$ (here m is in the range 1.7–2.0), while the average length L_w of sand waves is close to the wavelength λ that corresponds to the maximum ordinate of the spectrum (Grinvald & Nikora 1988). It is the second approach (sand waves as moving field of bottom elevations), considered to be of a more general and objective character, that will be used below.

3.1. *Correlation functions*

The analysis and interpretation of the full-dimensional correlation function $R(\Delta x, \Delta y, \tau)$ of the sand wave bottom involves certain difficulties. On the one hand, measuring bottom elevation fluctuations at many points in order to calculate $R(\Delta x, \Delta y, \tau)$ is technically difficult, especially in field conditions. On the other hand, it is difficult to provide a visual presentation of the three-dimensional correlation function $R(\Delta x, \Delta y, \tau)$ and, thus, to interpret it. A way out in this case is the obtaining and physical interpretation of linear and two-dimensional sections of the three-dimensional function $R(\Delta x, \Delta y, \tau)$. The schemes adopted for locating the micro-sounder radiators allowed us to obtain and investigate the following sections of function $R(\Delta x, \Delta y, \tau)$:

$R(0, 0, \tau)$ – time auto-correlation function;
$R(\Delta x, 0, 0)$ – longitudinal spatial auto-correlation function;
$R(0, \Delta y, 0)$ – transverse spatial auto-correlation function;
$R(\Delta x, 0, \tau)$ – longitudinal space–time correlation function, which may also be regarded as a longitudinal time cross-correlation function $R_{ij}(\tau)$ at distance Δx between measurement points i and j;

https://doi.org/10.1017/S0022112097006708 Published online by Cambridge University Press

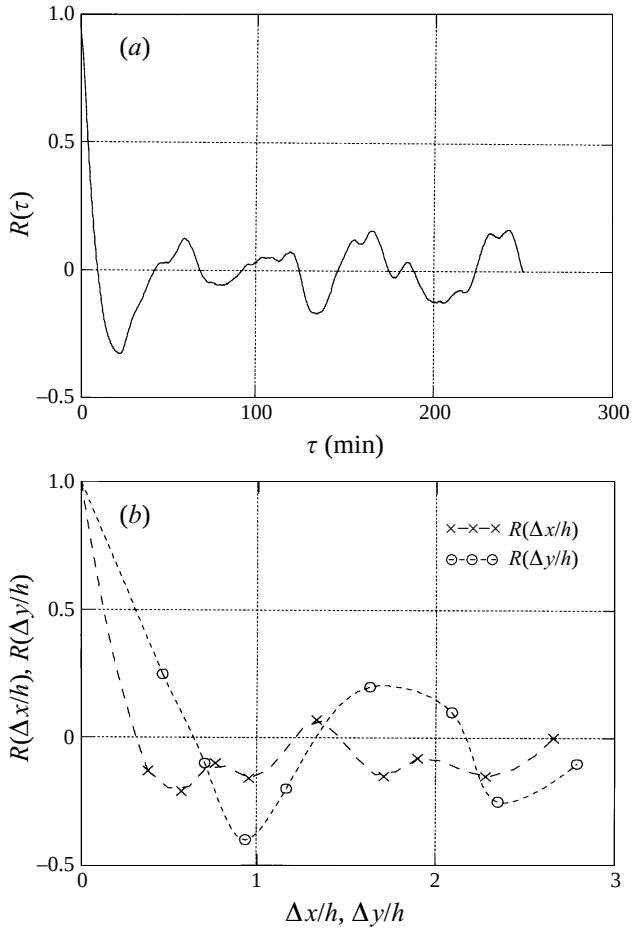


FIGURE 5. Examples of auto-correlation functions of sand waves for the Wilga River (Poland): (*a*) $R(\tau)$, (*b*) $R(\Delta x/h)$, $R(\Delta y/h)$ (h is the time-averaged depth over measured sand waves).

$R(0, \Delta y, \tau)$ – transverse space–time correlation function, which may also be regarded as a transverse time cross-correlation function $R_{ij}(\tau)$ at distance Δy between measurement points i and j.

The calculated time auto-correlation functions $R(\tau)$ of bottom fluctuations resemble a damped oscillation and, to a first approximation, they can be described by relationship $R(\tau) = \mathrm{e}^{-\alpha|\tau|} \cos 2\pi\tau/T$. The prevailing periods T of fluctuations of the functions $R(\tau)$ obtained, which characterize the time scales of moving sand waves, are typically 45–60 min for the Wilga River (Poland), 150–200 min for the Tirnava Mica River (Romania) and 90–170 min for the Buzau River (Romania).

The longitudinal and transverse spatial correlation functions $R(\Delta x)$ and $R(\Delta y)$ have shapes similar to that of $R(\tau)$. The spatial scales of sand waves in longitudinal and transverse directions, revealed on the graphs of functions $R(\Delta x)$ and $R(\Delta y)$ as characteristic wavelengths of their prevailing fluctuations, are approximately equal: 1.1–6.0 and 1.3–3.7 flow depths, respectively. Thus, the sand waves of all three experimental river reaches investigated are characterized by substantial three-dimensionality. Examples of functions $R(\tau)$, $R(\Delta x)$ and $R(\Delta y)$ are given in figure 5. Longitudinal and transverse space–time correlation functions $R(\Delta x, 0, \tau)$ and $R(0, \Delta y, \tau)$

https://doi.org/10.1017/S0022112097006708 Published online by Cambridge University Press

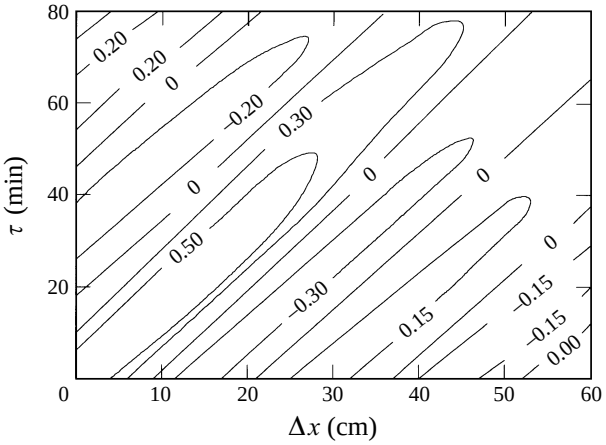


FIGURE 6. Topography of longitudinal space–time correlation function $R(\Delta x, 0, \tau)$ of sand waves for the Wilga River (Poland).

also point to the above-mentioned space–time scales. The location of hills and depressions in the relief of function $R(0, \Delta y, \tau)$ has an intermittent structure, thereby reflecting the three-dimensional character of the sand waves. A peculiar feature of the relief of the longitudinal space–time correlation function $R(\Delta x, 0, \tau)$ is the central, highest, hill whose crest is oriented obliquely to the Δx-axis (figure 6). In other words, the time shift, which corresponds to the maxima of the longitudinal time cross correlation function $R_{ij}(\tau)$, increases linearly with the distance Δx between measuring verticals.

3.2. *Structure functions*

Nikora (1982) and Robert & Richards (1988) first used structure functions for modelling the statistical properties of sand wave bottom longitudinal profiles. In this work we have investigated the time $D(0, 0, \tau)$ and spatial $D(\Delta x, 0, 0)$, $D(0, \Delta y, 0)$ sections of the three-dimensional structure function $D(\Delta x, \Delta y, \tau)$ defined by

$$D(\Delta x, \Delta y, \tau) = \overline{[Z(x+\Delta x, y+\Delta y, t+\tau) - Z(x, y, t)]^2} \tag{9}$$

where the overbar denotes the averaging operator over space and time.

Examples of the measured structure functions are given in figure 7. A characteristic feature of the time structure function $D(\tau)$ is the existence of two scaling regions with the exponent close to 1.0 at small τ and with the exponent in the range 1.6–2.0 in the region of intermediate τ. These features were revealed for all three experimental river reaches. The longitudinal spatial structure function $D(\Delta x)$ is also characterized by a scaling form at small Δx, with the scaling exponent close to 2.0 (figure 7). The same result for $D(\Delta x)$ was obtained earlier by Nikora (1982) in his analyses of the longitudinal profiles of sand waves in some rivers in the former USSR.

The transverse structure function $D(\Delta y)$ reflects the three-dimensional structure of the sand wave field: its ordinates increase with the growth of the three-dimensionality degree. In the region of small Δy, the empirical functions $D(\Delta y)$ obtained can be approximated by power functions with exponents 1.1 (Wilga, Poland), 1.25 (Tirnava Mica, Romania, figure 7) and 1.9 (Buzau, Romania). One can see that in contrast to temporal and spatial longitudinal structure functions, the scaling of $D(\Delta y)$ is far from being universal.

https://doi.org/10.1017/S0022112097006708 Published online by Cambridge University Press

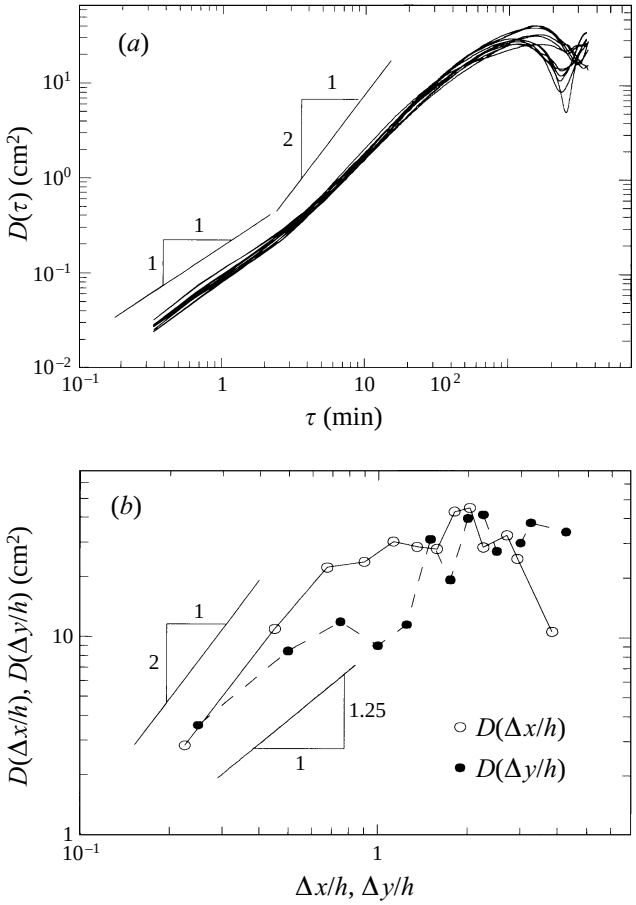


FIGURE 7. Examples of structure functions $D(\tau)$ (*a*) and $D(\Delta x/h)$, $D(\Delta y/h)$ (*b*), for the Tirnava Mica River, Romania (h is the time-averaged depth over measured sand waves).

The sections of the three-dimensional structure function $D(\Delta x, \Delta y, \tau)$ described contain information not only on the sand wave geometry, but also on their kinematics. Below, we shall show the relation between functions $D(\Delta x)$ and $D(\tau)$ which will be used in the next section for analysing the dispersity of sand waves.

Let us fix the elevation Z_0 of a point on the surface of a moving sand wave and watch the motion of this point. Assuming that the point moves only in the longitudinal direction and taking into account that $Z_0 = \text{const}$, we can write

$$\mathrm{d}Z_0 = \left.\frac{\partial Z}{\partial x}\right|_{Z_0} \mathrm{d}x + \left.\frac{\partial Z}{\partial t}\right|_{Z_0} \mathrm{d}t = 0. \tag{10}$$

The finite difference approximation gives

$$\Delta Z(\Delta x) = -\Delta Z(\Delta t). \tag{11}$$

Squaring and averaging both parts of equation (11) over all points of the longitudinal profile and time, we obtain the relationship

$$D(\Delta x) = D(\tau) \tag{12}$$

relating the longitudinal and time structure functions (for convenience we have

https://doi.org/10.1017/S0022112097006708 Published online by Cambridge University Press

substituted Δt by τ). At small enough Δx and τ the functions $D(\Delta x)$ and $D(\tau)$ can be expressed by scaling relationships

$$D(\Delta x) = a_x \Delta x^{2H_x}, \quad H_x \approx 1.0, \tag{13}$$

$$D_1(\tau) = a_{t1} \tau^{2H_{t1}}, \quad H_{t1} \approx 0.5, \quad \tau < \tau_0, \tag{14}$$

$$D_2(\tau) = a_{t2} \tau^{2H_{t2}}, \quad H_{t2} \approx 0.8\text{–}1.0, \quad \tau > \tau_0. \tag{15}$$

In relationships (13)–(15) a_x, a_{t1}, and a_{t2} are some coefficients, H_x, H_{t1}, and H_{t2} are Hurst's exponents whose numerical values were obtained from experiments, and τ_0 is the argument of the time structure function dividing the scaling regions (14) and (15).

It follows from (12)–(15) that

$$a_x \Delta x^{2H_x} = a_{t1} \tau^{2H_{t1}}, \quad \tau < \tau_0, \tag{16}$$

$$a_x \Delta x^{2H_x} = a_{t2} \tau^{2H_{t2}}, \quad \tau > \tau_0. \tag{17}$$

Relationships (16) and (17) constitute an analytical basis for replacing the variables when passing from the time structure functions to the spatial longitudinal ones and vice versa:

$$D(\tau) = D((a_x/a_t)^{1/(2H_t)} \Delta x^{H_x/H_t}), \tag{18}$$

$$D(\Delta x) = D((a_t/a_x)^{1/(2H_x)} \tau^{H_t/H_x}). \tag{19}$$

3.3. *Sand wave spectra*

The correlation function $R(\Delta x, \Delta y, \tau)$ and the three-dimensional spectrum $S(K_x, K_y, \omega)$ contain the same information concerning the properties of the random field $Z(x, y, t)$ and thus they are of equal value. However, the spectral description of the field $Z(x, y, t)$ in the frequency–wavenumber space is often more vivid and convenient for analysis and interpretation.

Here we shall consider the projection of the three-dimensional spectrum $S(K_x, K_y, \omega)$ on the axes K_x, K_y, and ω:

$$S(K_x) = \int\int_0^{+\infty} S(K_x, K_y, \omega)\, \mathrm{d}K_y\, \mathrm{d}\omega, \tag{20}$$

$$S(K_y) = \int\int_0^{+\infty} S(K_x, K_y, \omega)\, \mathrm{d}K_x\, \mathrm{d}\omega, \tag{21}$$

$$S(\omega) = \int\int_0^{+\infty} S(K_x, K_y, \omega)\, \mathrm{d}K_x\, \mathrm{d}K_y. \tag{22}$$

To determine $S(K_x)$, $S(K_y)$ and $S(\omega)$ from our field data we used Fourier transformation of linear sections of the correlation function $R(\Delta x, \Delta y, \tau)$ on axes $\Delta x, \Delta y$ and τ together with Tukey's correlation window (Bath 1974). Examples of functions $S(K_x)$, $S(K_y)$ and $S(\omega)$ are shown in figure 8. All the $S(K_x)$ and $S(\omega)$ spectra studied are characterized by scaling regions where the spectral density decreases according to power law with the exponent close to -3. A second scaling region with the exponent close to -2 (figure 8) can be also distinguished in the high-frequency region of the frequency spectra. Such behaviour is in good agreement with frequency spectra of flume sand waves, given in Shen & Cheong (1977) (see the Introduction). Both cases show behaviour (-2 for high frequencies and -3 for low frequencies) contrary to that established by Hino (1968). A possible explanation of this discrepancy is that Hino's (1968) results were obtained from very limited data with poor frequency resolution. The $S(K_y)$ spectra also show that at large K_y they can be described by a power function. However, the power

https://doi.org/10.1017/S0022112097006708 Published online by Cambridge University Press

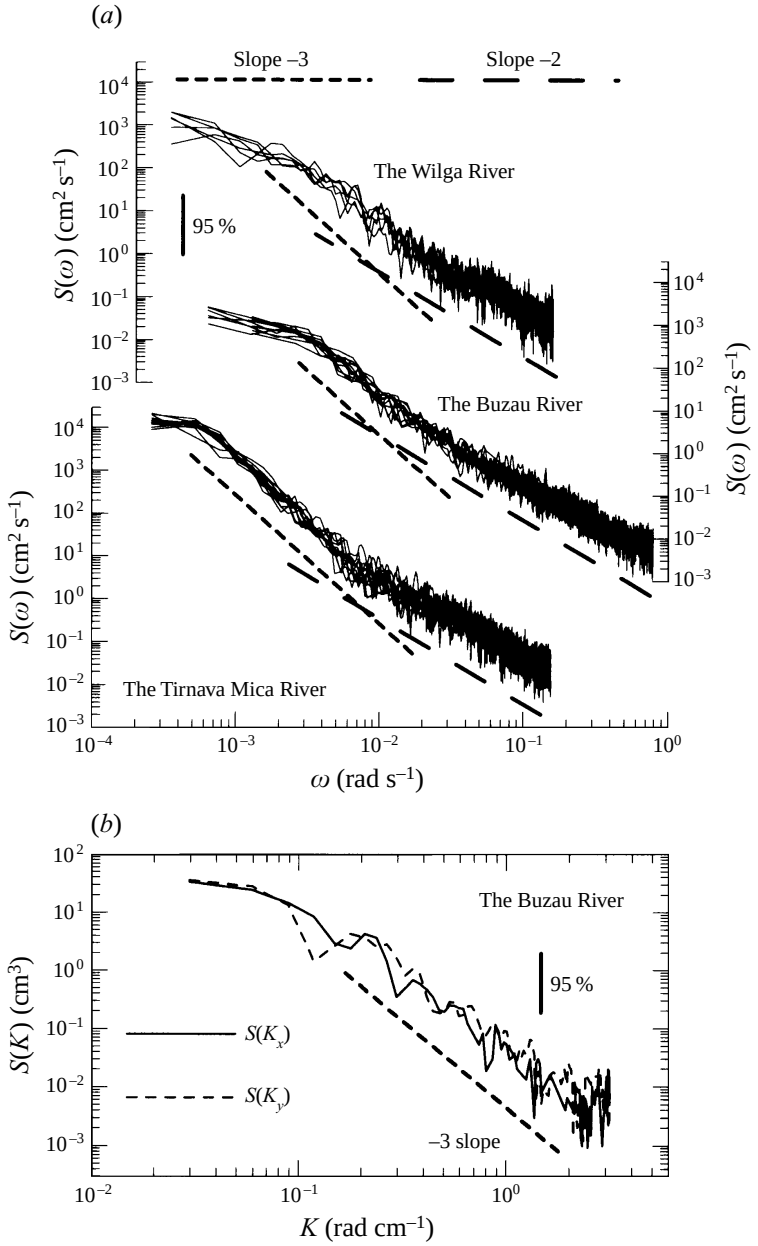


FIGURE 8. Examples of sand wave spectra: (*a*) frequency spectra $S(\omega)$, and (*b*) wavenumber spectra $S(K_x)$ and $S(K_y)$.

exponents display rather strong differences from site to site: 2.1 for Wilga (Poland), 2.3 for Tirnava Mica (Romania) and 2.9 for Buzau (Romania).

These results provide grounds for presenting scaling spectra, $S(K_x)$, $S(K_y)$, and $S(\omega)$, as follows:

$$S(K_x) = A_x K_x^{-(2H_x+1)}, \quad H_x \approx 1.0, \quad K_x > K_{x0}, \tag{23}$$

$$S(K_y) = A_y K_y^{-(2H_y+1)}, \quad H_y \approx 0.5\text{–}1.0, \quad K_y > K_{y0}, \tag{24}$$

$$S_1(\omega) = A_{t1}\omega^{-(2H_{t1}+1)}, \quad H_{t1} \approx 0.5, \quad \omega_1 < \omega < \omega_\infty, \tag{25}$$

$$S_2(\omega) = A_{t2}\omega^{-(2H_{t2}+1)}, \quad H_{t2} \approx 1.0, \quad \omega_0 < \omega < \omega_1, \tag{26}$$

https://doi.org/10.1017/S0022112097006708 Published online by Cambridge University Press

where A_x, A_y, A_{t1} and A_{t2} are some coefficients, H_x, H_y. H_{t1} and H_{t2} are exponents that characterize the structure of bottom elevation fluctuations, and $K_{x0}, K_{y0}, \omega_0, \omega_1, \omega_\infty$ are boundary wavenumbers and frequencies, respectively. The values of H_j are in good agreement with those obtained on the basis of the structure functions analysis, relationships (13)–(15).

3.4. *Sand wave dispersion relation*

The velocity of sand wave propagation is an important kinematic characteristic that determines the intensity of bed sediment transport. All existing formulae for calculating the bottom sediment discharge using bathymetric data are based on the supposition that sand waves propagate without changing their shape, at least from the statistical point of view (Shen & Cheong 1977; Engel & Lau 1980; Cheong 1992). The use of this assumption is equal to adopting the hypothesis that sand waves are non-dispersive, i.e. their velocity C is independent of their wavelengths. However, the theoretical analysis (Cartwright 1959; Kennedy 1963, 1969; Reynolds 1965; Gradowczyk 1968; Jain & Kennedy 1974; Engelund & Fredsoe 1982) and some experimental data (Hino 1968; Shen & Cheong 1977) point to the existence of sand wave dispersion, at least within some scale ranges. In view of the importance of this question for sediment transport analysis, we shall proceed with the study of this problem based on the obtained experimental data. We shall apply three approaches: (i) analysis of the structure functions, (ii) analysis of the frequency spectra and (iii) the method of cross-correlation functions.

3.4.1. *Analysis of structure functions*

Relationships (16) and (17) constitute the theoretical basis for our analysis. Let us transform them as follows:

$$C(\Delta x) = \frac{\Delta x}{\tau} = \left(\frac{a_{t1}}{a_x}\right)^{1/(2H_{t1})} \Delta x^{(H_{t1}-H_x)/H_{t1}}, \quad \tau < \tau_0, \tag{27}$$

$$C(\Delta x) = \frac{\Delta x}{\tau} = \left(\frac{a_{t2}}{a_x}\right)^{1/(2H_{t2})} \Delta x^{(H_{t2}-H_x)/H_{t2}}, \quad \tau > \tau_0. \tag{28}$$

Substituting numerical values of the exponents H_i into (27) and (28) yields

$$C(\Delta x) \propto \Delta x^{-1}, \quad \tau < \tau_0, \tag{29}$$

$$C(\Delta x) \propto \Delta x^{-(0\text{–}0.25)}, \quad \tau > \tau_0. \tag{30}$$

The time scale τ_0 separating two zones – with dispersion (29) and without dispersion (30) – corresponds to wavelengths in the range $0.15h$ to $0.25h$, where h is the time-averaged depth over measured sand waves. To get the above range we used relationships (16) and (17) whence it follows that

$$(\Delta x \text{ or } \lambda)/h = (a_{t1}/a_x)^{1/(2H_x)}\, \tau_0^{H_{t1}/H_x}/h = (a_{t2}/a_x)^{1/(2H_x)}\, \tau_0^{H_{t2}/H_x}/h.$$

3.4.2. *Analysis of frequency spectra*

The longitudinal wavenumber $S(K_x)$ and the frequency $S(\omega)$ spectra can be related as

$$S(K_x)\,\mathrm{d}K_x = S(\omega)\,\mathrm{d}\omega. \tag{31}$$

From (23), (25), (26) and (31), after integration we obtain

$$C(K_x) = \frac{\omega}{K_x} \propto K_x^{(H_x-H_{t1})/H_{t1}}, \quad \omega_1 < \omega < \omega_\infty, \tag{32}$$

$$C(K_x) = \frac{\omega}{K_x} \propto K_x^{(H_x-H_{t2})/H_{t2}}, \quad \omega_0 < \omega < \omega_1. \tag{33}$$

https://doi.org/10.1017/S0022112097006708 Published online by Cambridge University Press

Substituting the numerical values of the exponents H_x, H_{t1} and H_{t2} from the previous section into (32) and (33) gives

$$C(K_x) \propto K_x, \quad \omega_1 < \omega < \omega_\infty, \tag{34}$$

$$C(K_x) \propto K_x^0, \quad \omega_0 < \omega < \omega_1. \tag{35}$$

As for the case of the structure functions, the estimation of wavelengths corresponding to the boundary frequency ω_1 produces (0.15–0.25) h.

3.4.3. *Method of cross-correlation functions*

The method of cross-correlation functions can be regarded as a direct one. Its detailed description and substantiation is given by Bendat & Piersol (1980). The essence of this method is in the estimation of the time shift τ_m that corresponds to the maximum ordinate of the longitudinal cross-correlation function $R_{ij}(\tau)$ at fixed Δx (it is worth pointing out that function $R_{ij}(\tau)$ may be regarded as a linear section of the function $R(\Delta x, 0, \tau)$ at given Δx). The velocity of sand waves is then determined from $C = \Delta x/\tau_m$. Carrying out a consecutive band filtration of bottom elevation time series and applying the described method to filtered series we can determine if the velocity of sand waves depends on their period or on their wavelength. For the band filtration we have utilized the Tukey cosine-filter (Bendat & Piersol 1980).

Figure 9(*a*) shows the results of calculations for all three river reaches on the Wilga (Poland), Tirnava Mica (Romania) and Buzau (Romania) Rivers. To eliminate the substantial stratification of the experimental points on graph $C = f(\lambda)$, we have studied various approaches for normalizing the velocity C and the length λ of the sand waves. The most successful of our attempts are given in figures 9(*b*) and 9(*c*). These are based on the relationship of Snishchenko & Kopaliani (1978)

$$C = 0.019u\,Fr^{2.9} \tag{36}$$

that was obtained from many laboratory and field data and from the assumption of non-dispersity of sand waves. Taking into account that relationship (36) characterizes the velocity of prevailing sand waves whose lengths are, as a rule, larger than the flow depth (Snishchenko & Kopaliani 1978), we have proposed a more general form

$$C = u\,Fr^{2.9} f\left(\frac{g\lambda}{u^2 \text{ (or } u_*^2)}\right), \tag{37}$$

where u_* is the friction velocity (to test relationship (37) we defined the friction velocity by $u_* = (\tau_{s0}/\rho)^{1/2} = (ghI)^{1/2}$, where h is the time-averaged depth over measured sand waves, I is the water surface slope, and τ_{s0} is the bed shear stress, table 1), and u is the vertically averaged flow velocity. At large $g\lambda/u^2$ or $g\lambda/u_*^2$, we expect that the function $f(g\lambda/u^2$ (or $u_*^2))$ tends to a constant value equal to 0.019, and a relationship (37) becomes identical to (36). At small $g\lambda/u^2$ or $g\lambda/u_*^2$ the function $f(g\lambda/u^2$ (or $u_*^2))$ tends to the power function with exponent -1. To some extent figures 9(*b*) and 9(*c*) confirm our hypothesis. As the first approximation for small wavelengths we can write

$$C = 0.66u\,Fr^{2.9}(g\lambda/u^2)^{-1} \tag{38}$$

or, when using u_*,

$$C = 86u\,Fr^{2.9}(g\lambda/u_*^2)^{-1}. \tag{39}$$

Unlike the structure functions and spectra, which allowed us to consider the dispersion relation for small wavelengths, the resolving power of the cross-correlation functions method is substantially lower. This is restricted by minimum distances between the microsound radiators. We believe that this explains the region in figures 9(*b*) and 9(*c*)

https://doi.org/10.1017/S0022112097006708 Published online by Cambridge University Press

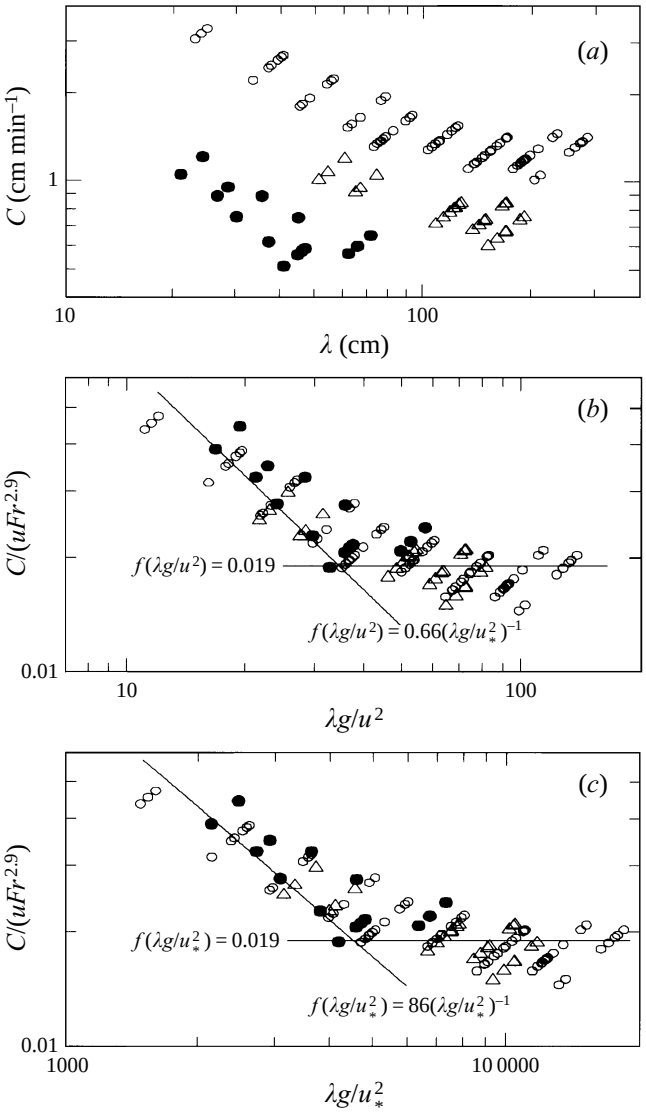


FIGURE 9. Graphs of $C = f(\lambda)$ (*a*), $C/(uFr^{2.9}) = F(g\lambda/u^2)$ (*b*), and $C/(uFr^{2.9}) = f(g\lambda/u_*^2)$ (*c*) for the Wilga River (squares), the Tirnava Mica River (triangles) and the Buzau River (circles). To test relationship (37) we defined friction velocity by $u_* = (ghI)^{1/2}$, where h is the time-averaged depth over measured sand waves, I is the water surface slope.

where $C \propto K_x$ is not distinguished clearly. The minimum wavelengths shown in figures 9(*b*) and 9(*c*) exceed $0.8h$, while from the analysis of structure functions and spectra the dispersive region with $C \propto K_x$ corresponds to scales that are less than (0.15–0.25) h. Probably, in figures 9(*b*) and 9(*c*) we have only the transition zone between the regions with $C \propto K_x$ and $C \propto K_x^0$, as well as the region with $C \propto K_x^0$. Hence, relationships (38) and (39) should be regarded as preliminary, requiring verification.

Thus, all three approaches provide results which are in qualitative agreement: in the region of small wavelengths, at $\lambda \leqslant (0.15\text{–}0.25)\,h$, one can observe the dispersion of sand waves in the form of $C \propto K_x$; while in the lower-frequency region, $\lambda \geqslant (3\text{–}4)\,h$, the sand waves show no significant dispersion, i.e. $C \propto K_x^0$.

https://doi.org/10.1017/S0022112097006708 Published online by Cambridge University Press

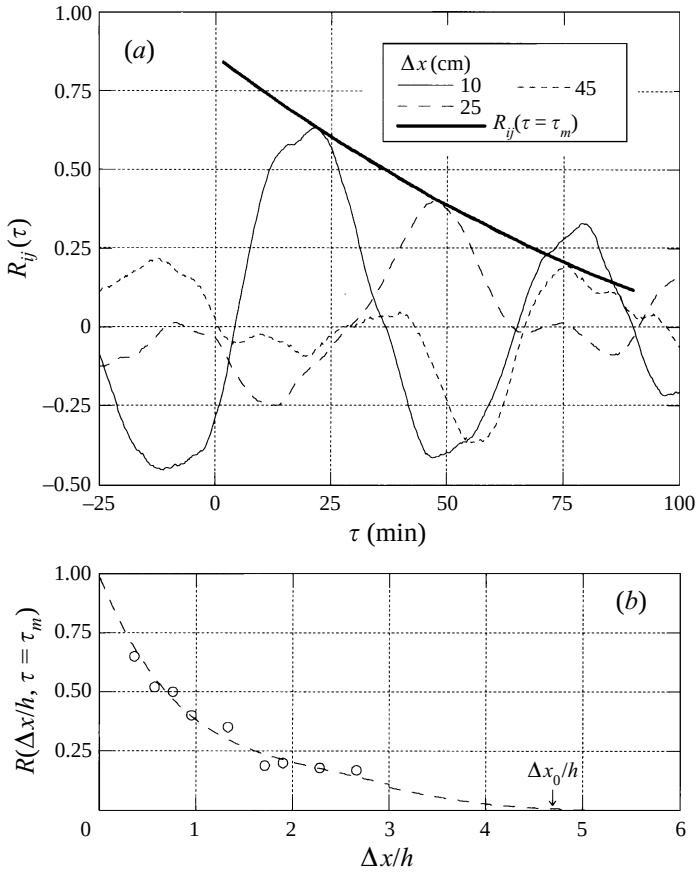


FIGURE 10. Longitudinal time cross-correlation function $R_{ij}(\tau)$ (*a*) and function $R(\Delta x/h, \tau = \tau_m)$ (*b*), for the Wilga River, Poland (h is the time-averaged depth over measured sand waves).

Probably, the sand wave dispersion in the ranges considered is a possible reason for the substantial deformation observed in individual sand waves in the process of their movement. It is clearly expressed in the rapid deformation of the cross-correlation functions $R_{ij}(\tau)$ with the increase of the distance Δx between measuring verticals (figure 10). When the sand wave field is totally non-dispersive and Δx changes, the curve $R_{ij}(\tau)$ must shift to the right without modifying its form. However, in a real situation, we observe deformation of $R_{ij}(\tau)$: when Δx increases, the maximum ordinate of $R_{ij}(\tau)$ decreases (figure 10*a*). Having defined the Δx_0 at the zero value of $R_{ij}(\Delta x, \tau = \tau_m)$ where τ_m corresponds to the maximum ordinate of the longitudinal cross-correlation function $R_{ij}(\tau)$ at fixed Δx, we can approximately estimate the distance over which the total loss of sand wave individuality occurs. By extrapolating the curve $R_{ij}(\Delta x, \tau = \tau_m)$ in figure 10(*b*) towards increasing Δx, we find $\Delta x_0 \approx (4\text{–}6)\,h$. Thus, having moved a distance of several wavelengths, the sand waves lose their individual properties completely.

3.4.4. *Discussion*

From the existing theoretical considerations (Cartwright 1959; Kennedy 1963, 1969; Reynolds 1965; Gradowczyk 1968; Jain & Kennedy 1974; Engelund & Fredsoe 1982) it follows that for sufficiently large wavenumbers we have $C \propto K_x \propto \lambda^{-1}$ while for the region of small wavenumbers no significant dispersion occurs. Hino (1968) used the

https://doi.org/10.1017/S0022112097006708 Published online by Cambridge University Press

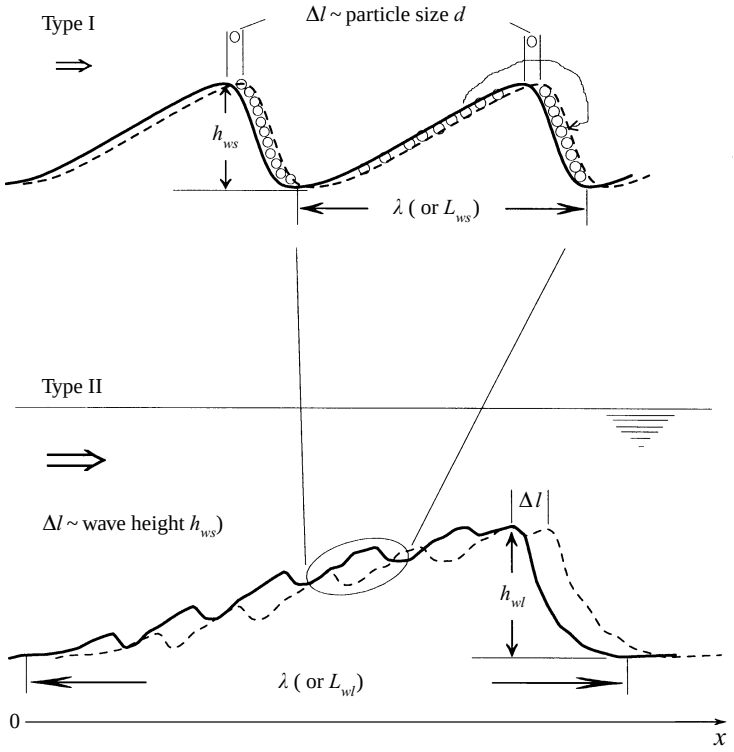


FIGURE 11. Two types of sand wave movement.

relation $C \propto K_x \propto \lambda^{-1}$ to derive relation (3), $S(\omega) \propto \omega^{-2}$, from $S(K_x) \propto K_x^{-3}$. At the same time, for the region of higher frequencies he suggested that both frequency and wavenumber spectra have the same exponent -3. This automatically means non-dispersity of small sand waves, and that does not agree with either the existing theory or our measurements. In spite of our experimental results proving to be consistent with the theoretical predictions we cannot be fully satisfied. The reasons for this are: (i) the above theoretical models are based on a number of assumptions (potential flow, perturbations of small amplitude, etc.) that restrict their applicability to the case of fully developed sand waves (McLean 1990); and (ii) they do not consider physical mechanisms of sand wave movement. However, we believe that the mechanisms of sand wave movement can be a possible explanation of the observed sand wave dispersion.

Based on numerous observations of sand waves in rivers, two types of sand wave movement can be distinguished (figure 11). The first type (I) is for the region of large wavenumbers (small wavelengths) and the second one (II) is for the region of small wavenumbers (large wavelengths). The small sand waves move due to the motion of individual sand particles (type I, figure 11) while larger sand waves propagate as a result of the motion of smaller waves on their upstream slopes (type II, figure 11). In the same manner as sand particles in the first type, these smaller waves redistribute sand material from upstream slopes to downstream ones. Both types result in sand wave movement downstream. We will use these considerations to obtain the dispersion relation.

In general, the propagation velocity of an individual sand wave is

$$C = \Delta l / \Delta t, \tag{40}$$

https://doi.org/10.1017/S0022112097006708 Published online by Cambridge University Press

where Δl is the distance the sand wave moves in time Δt. Applying relationship (40) for the case of small sand waves (type I) and assuming, reasonably, $\Delta t \propto Nd \propto h_w \propto \lambda$ (N is the number of particles of size d covering the downstream slope of a sand wave) when $\Delta l \propto d$ (figure 11) we have

$$C \propto d/\lambda \propto \lambda^{-1} \propto K_x. \tag{41}$$

The reason to assume that sand wave height $h_w \propto$ sand wavelength λ is based on the self-similar spectrum $S(K_x) \propto K_x^{-3}$ that reflects statistical self-similarity of sand waves (Hurst exponent $H_x = 1$, see the Introduction). So, for the case of the small waves, dispersion relation (41), $C \propto K_x \propto \lambda^{-1}$, should be expected. Indeed, we found this from the experiments. For large sand waves (type II), it is natural to assume $\Delta t \propto h_{wl}$ when $\Delta l \propto h_{ws}$, where h_{ws} is the height of small sand waves moving on the upstream slope of large waves of height h_{wl} (figure 11). Using a spectral representation, the heights h_{wl} and h_{ws} can be expressed as $h_{ws} \propto \{S(K_{xs})\,\mathrm{d}K_x\}^{1/2}$ and $h_{wl} \propto \{S(K_{xl})\,\mathrm{d}K_x\}^{1/2}$, respectively. With this their propagation velocity will be

$$C \propto \frac{h_{ws}}{h_{wl}} \propto \frac{\{S(K_{xs})\,\mathrm{d}K_x\}^{1/2}}{\{S(K_{xl})\,\mathrm{d}K_x\}^{1/2}} \propto \frac{\{S(K_{xs})\,\mathrm{d}K_x\}^{1/2}}{\{S(nK_{xs})\,\mathrm{d}K_x\}^{1/2}} \propto K_x^0 \propto \text{const}, \tag{42}$$

where $S(K_x) \propto K_x^{-3}$, and $n < 1$. From relationship (42) the large sand waves should move without dispersion. This was observed in our experiments. For the case of our study, the relationship $C \propto K_x \propto \lambda^{-1}$ is valid when $\lambda < (0.15\text{–}0.25)\,h$, and no significant dispersion occurs at $\lambda \geqslant (3\text{–}4)\,h$.

The above scaling consideration significantly simplifies the process, which is much more complex in reality. A new insight into the problem should be obtained by finite-amplitude models that couple wakes and boundary layers over sand waves with mechanisms of sand transport. Such models are being developed but they still need to be improved (McLean 1990).

4. Some properties of the flow turbulence over moving sand waves

To evaluate the properties of the flow turbulence over the sand waves investigated, we carried out joint measurements of instantaneous velocities and bottom elevations at fixed verticals on the Wilga River (Poland) and on the Tirnava Mica River (Romania). The total duration of measurements was 4 h (Wilga) and 6.5 h (Tirnava Mica). The bottom elevations were measured every 2 min. Velocity measurements were made at three (Wilga) and six (Tirnava Mica) points simultaneously in the $Z/h =$ 0.29–0.96 layer in separate series of 4–5 min each. The sampling interval was 0.1 s (Wilga) and 0.075 s (Tirnava Mica). The breaks between series of velocity measurements ranged within 10 to 15 min. Taking account of the space–time scales of bottom elevation fluctuations given in the previous sections, the scheme of measurements adopted allowed us to obtain a set of quasi-stationary time series of velocities that correspond to various phases of sand waves. From the measured data, we calculated the local mean velocity $\bar{U}$, the velocity variance σ_u^2, the turbulence intensity $K = \sigma_u/\bar{U}$, the correlation functions and frequency spectra, and the turbulent energy dissipation ϵ for each time series. The limited number of measuring points precludes a detailed characterization of the turbulence structure over sand waves. More detailed pictures are given in the works of Smith & McLean (1977), McLean & Smith (1979), Nikora (1985), Grinvald & Nikora (1988), Nelson, McLean & Wolfe (1993), McLean, Nelson & Wolfe (1994). Therefore, here we shall limit ourselves to the quantitative estimation of the modulating influence of sand waves upon turbulence.

https://doi.org/10.1017/S0022112097006708 Published online by Cambridge University Press

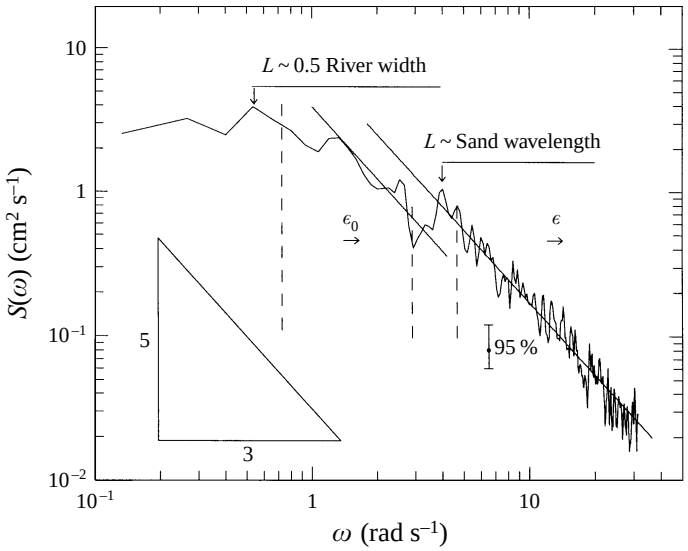


FIGURE 12. Example of a longitudinal velocity frequency spectrum for the Wilga River (Poland).

$\overline{\overline{z}}/\overline{\overline{h}}$	$\overline{\overline{U}}$ (m s^{-1})	$\frac{\sigma_{\overline{u}}}{\overline{\overline{U}}}$	$\overline{\overline{\sigma_u^2}}$ (cm^2 s^{-2})	$\frac{\sigma_{\sigma_u^2}}{\overline{\overline{\sigma_u^2}}}$	$\overline{\overline{K}}$	$\frac{\sigma_K}{\overline{\overline{K}}}$	$\overline{\overline{\epsilon}}$ (cm^2 s^{-3})	$\frac{\sigma_\epsilon}{\overline{\overline{\epsilon}}}$
The Wilga River (Poland), $\overline{\overline{h}} = 0.255$ m								
0.30	0.34	0.047	20.1	0.14	0.130	0.09	6.9	0.24
0.53	0.37	0.031	10.5	0.12	0.088	0.09	2.0	0.18
0.76	0.39	0.030	8.5	0.12	0.076	0.08	1.3	0.18
The Tirnava Mica River (Romania), $\overline{\overline{h}} = 0.374$ m								
0.29	0.44	0.082	29.2	0.16	0.130	0.07	9.7	0.25
0.37	0.51	0.061	33.1	0.13	0.121	0.08	6.6	0.19
0.49	0.53	0.056	24.5	0.16	0.094	0.07	5.3	0.22
0.65	0.54	0.037	18.3	0.16	0.083	0.06	2.1	0.20
0.81	0.57	0.035	13.1	0.14	0.063	0.06	0.52	0.16
0.96	0.55	0.036	7.4	0.19	0.050	0.05	0.45	0.24

TABLE 3. Turbulence characteristics and their variability. Here $\overline{\overline{h}}$ is the flow depth averaged over the whole period of measurements; $\overline{\overline{z}}$ is the average distance from the bottom; K is the turbulence intensity, $K = \sigma_u/\bar{u}$; $\sigma_{\bar{u}}$, σ_{σ^2}, σ_K, and σ_ϵ are standard deviations of local mean velocity, turbulence energy, turbulence intensity, and turbulent energy dissipation, respectively; and the double overbar denotes the averaging of the values obtained for each separate velocity time series.

Table 3 shows the turbulence characteristics averaged with respect to all time series, as well as their relative variation conditioned by sand waves passing through the measuring vertical. The averaged velocities show the least variation (3–8.2 %). The turbulence energy σ_u^2 and the turbulence intensity K are characterized by higher variability, reaching 5–19 % (table 3).

In frequency spectra of longitudinal velocities, despite relatively small Reynolds numbers, one can observe wide ranges of frequencies corresponding to the inertial subrange (figure 12)

$$S(\omega) = c\bar{U}^{2/3}\epsilon^{2/3}\omega^{-5/3}. \tag{43}$$

Two frequency ranges described by (43) occur in practice on all of the spectra obtained.

https://doi.org/10.1017/S0022112097006708 Published online by Cambridge University Press

These are separated by the local spectral maximum, which can be interpreted as an additional energy supply region caused by the interaction between flow and sand waves (Grinvald & Nikora 1988). The spatial scale corresponding to this energy supply region is close to the length of prevailing sand waves (figure 12).

The low-frequency boundary of the left-side inertial subrange corresponds to 8–9 flow depths or to half of the river width. Thus, applying (43) we can determine the inflow of energy ϵ_0 into the turbulence spectrum as a result of hydrodynamic instability on scales of the river half-width (the left-side inertial subrange), as well as the turbulent energy dissipation ϵ (using the right-side inertial subrange) and the quantity of energy inflow due to the influence of sand waves $\Delta\epsilon = \epsilon - \epsilon_0$ (figure 12). Table 3 shows the $\bar{\epsilon}$ values averaged in respect to all time series, as well as the variation in ϵ caused by the passing sand waves. It follows from table 3 that this characteristic is subjected to the strongest influence of sand waves, varying in the range from 16% to 25%. The contribution of sand wave influence upon the whole turbulence energy flux $\Delta\epsilon/\epsilon_0$ varies from 3 to 8, thus providing grounds for considering the sand waves as the main mechanism to regulate the energy losses of the flow. The above-mentioned quantitative parameters of turbulence characterize the intermediate region of the flow. It is obvious that in the region near the bottom the influence of sand waves is considerably stronger.

5. Summary

Longitudinal wavenumber spectra of sand waves in the region of large wavenumbers follow Hino's -3 law ($S(K_x) \propto K_x^{-3}$) quite satisfactorily, confirming the theoretical predictions of Hino (1968) and Jain & Kennedy (1974). At the same time, frequency-spectra scaling behaviour proved to be quite different from the earlier results of Hino (1968), who found two frequency regions, with scaling exponents -3 for large frequencies and -2 for smaller ones. Our results also showed two scaling regions but with exponents -2 for large frequencies and -3 for smaller ones. The transverse wavenumber spectra of sand waves can be described at large wavenumbers by a power function; however, the scaling exponents appeared to vary from one river reach to another. Analysis of time and spatial structure functions showed similar scaling behaviour.

Three methods for investigating dispersion properties of sand waves (structure functions, spectral analysis and cross-correlation functions) produced the same result: in the region of small wavelengths ($\lambda \ll h$) dispersion ($C \sim K \sim \lambda^{-1}$) occurs, while in the region of large wavelengths ($\lambda \gg h$), dispersion is practically absent ($C \sim K^0 \sim \lambda^0$). This result also does not agree with Hino's (1968) analysis, but it is in satisfactory agreement with theoretical models (Kennedy 1963; Jain & Kennedy 1974) and with physical analysis of sand wave movement at small and large scales. The parametrization of the sand wave dispersion relation $C = f(\lambda)$ with vertically averaged flow velocity, depth Froude number, and wavelength Froude number significantly reduced the experimental point scatter. We believe that the dispersion relationships derived can be used for estimations of sediment transport by sand waves.

The modulating influence of sand waves on the average velocity and turbulence is reflected in their strong space–time variation: 3–8% for the local mean velocity, 12–19% for the turbulence energy, 5–9% for the turbulence intensity, and 16–25% for the turbulent energy dissipation.

This research was made possible by Grant No. RZCOOO from the International Science Foundation (to V. N.) and support from the National Institute of Water and

https://doi.org/10.1017/S0022112097006708 Published online by Cambridge University Press

Atmospheric Research (New Zealand), Institute of Geophysics and Geology (Moldova), and Institute of Geophysics (Poland). The authors are grateful to I. Ichim, N. Radoane, M. Radoane, G. Shalar, N. Arnaut, and J. Szkutnicki and his co-workers for their help in the field as well as to C. Paola, S. McLean, D. M. Hicks and G. Carter for useful discussions and comments. Three anonymous reviewers provided very thorough reviews and useful comments which helped the authors to improve the initial manuscript.

REFERENCES

Annambhotla, V. S., Sayre, W. W. & Livesey, R. H. 1972 Statistical properties of Missouri river bed forms. *J. Waterways, Harbors, Coast Eng. Div. ASCE* **98** (W4), 489–510.

Ashida, K. & Tanaka, Y. 1967 Experimental study on sand waves. *Disaster Prevention Res. Inst. Ann., Kyoto Univ.* **N10**, 121–132.

Baliga, B. R. & Hudspeth, R. T. 1981 Evaluation of sand waves in an estuary. *J. Hydraul. Div. ASCE* **107** (HY2), 161–178.

Bath, M. 1974 *Spectral Analysis in Geophysics*. Elsevier.

Bendat, J. S. & Piersol, A. G. 1980 *Engineering Applications of Correlation and Spectral Analysis*, Wiley-Interscience.

Cartwright, D. E. 1959 On submarine sand-waves and tidal lee-waves. *Proc. R. Soc., Lond.* A **253**, 218–241.

Cheong, H. F. 1992 Probability distribution of the speed of sediments and sediment waveforms. *J. Hydraul. Res.* **30**, 265–275.

Dinehart, R. L. 1989 Dune migration in a steep, coarse-bedded stream. *Water Resour. Res.* **25**, 911–923.

Engel, P. & Lau, Y. L. 1980 Computation of bed load using bathymetric data. *J. Hydraul. Div. ASCE* **106** (HY3), 369–380.

Engelund, F. & Fredsoe, J. 1982 Sediment ripples and dunes. *Ann. Rev. Fluid Mech.* **14**, 13–37.

Fukuoka, S. 1968 Generation, development and spectrum of sand waves. *Dep. Civ. Engng Tokyo Inst. Techn., Tech. Rep.* N4, pp. 44–55.

Gradowczyk, M. H. 1968 Wave propagation and boundary instability in erodible-bed channels. *J. Fluid Mech.* **33**, 93–112.

Grinvald, D. I. & Nikora, V. I. 1968 *River Turbulence*. Hydrometeoizdat, Leningrad (in Russian).

Hino, M. 1968 Equilibrium-range spectra of sand waves formed by flowing water. *J. Fluid Mech.* **34**, 565–573.

Jain, S. C. & Kennedy, J. F. 1974 The spectral evolution of sedimentary bedforms. *J. Fluid Mech.* **63**, 301–314.

Kennedy, J. F. 1963 The mechanics of dunes and antidunes in alluvial channels. *J. Fluid Mech.* **16**, 521–544.

Kennedy, J. F. 1969 The formation of sediment ripples, dunes and antidunes. *Ann. Rev. Fluid Mech.* **1**, 147–167.

Levey, R. A., Kjerfve, B. & Getzen, R. T. 1980 Comparison of bed form variance spectra within a meander bend during flood and average discharge. *J. Sediment. Petrol.* **50**, 149–155.

McLean, S. R. 1990 The stability of ripples and dunes. *Earth-Sci. Rev.* **29**, 131–144.

McLean, S. R., Nelson, J. M. & Wolfe, S. R. 1994 Turbulence structure over two-dimensional bed forms: Implications for sediment transport. *J. Geophys. Res.* **99** (C6), 12729–12747.

McLean, S. R. & Smith, J. D. 1979 Turbulence measurements in the boundary layer over a sand wave field. *J. Geophys. Res.* **84**, 7791–7808.

Mandelbrot, B. B. 1982 *The Fractal Geometry of Nature*. W. H. Freeman.

Monin, A. S. & Yaglom, A. M. 1975 *Statistical Fluid Mechanics*: Vol. 2, *Mechanics of Turbulence*. MIT Press.

Nelson, J. M., McLean, S. R. & Wolfe, S. R. 1993 Mean flow and turbulence fields over two-dimensional bed forms. *Water Resour. Res.* **29**, 3935–3953.

https://doi.org/10.1017/S0022112097006708 Published online by Cambridge University Press

NIKORA, V. I. 1982 Statistical peculiarities of river bed microforms (in Russian). In *Problems of Surface Hydrology*, pp. 143–151. Hydrometeoizdat, Leningrad.

NIKORA, V. I. 1983 Sand wave spectra in a translational flow. *Met. Hydrol.* **5**, 92–102 (in Russian).

NIKORA, V. I. 1985 On the structure of turbulence of river flows with sand wave bottom. *Met. Hydrol.* **6**, 74–84 (in Russian).

NIKORA, V. I. 1987 Spectral characteristics of laboratory microforms (sand waves). *Proc. State Hydrolog. Inst.* **307**, 63–70 (in Russian).

NIKORA, V. I., BORIK, S. A. & KUZMIN, V. F. 1988 On the spatial and time variability of the Lower Dniester hydraulic and morphological characteristics. *Prof. Paper GM-88*, *VNIIGMI-MCD*, *Obninsk*, *Russia*, pp. 1–27 (in Russian).

NIKORA, V. I., ROWINSKI, P. M., SUKHODOLOV, A. & KRASUSKI, D. 1994 Structure of river turbulence behind warm-water discharge. *J. Hydraul. Engng* **120**, 191–208.

NIKORA, V. I., SUKHODOLOV, A., SHALAR, G. & ROWINSKI, P. M. 1995 Field measurements of sand wave spectra in river. *Proc. 8th Intl Conf. on Transport and Sedimentation of Solid Particles*, Prague, pp. C5-1–C5-6.

NORDIN, C. F. 1971 Statistical properties of dune profiles. *US Geol. Survey Prof. Paper* 562F.

NORDIN, C. F. & ALGERT, J. H. 1966 Spectral analysis of sand waves. *J. Hydraul. Div. ASCE* **92** (HY5), 95–114.

REYNOLDS, A. J. 1965 Waves on the erodible bed of an open channel. *J. Fluid Mech.* **22**, 113–133.

ROBERT, A. & RICHARDS, K. S. 1988 On the modelling of sand bedforms using the semivariogram. *Earth Surface Processes and Landforms* **13**, 459–473.

SHEN, H. W. & CHEONG, H. F. 1977 Statistical properties of sediment bed profiles. *J. Hydraul. Div. ASCE* **103**, HY11, 1303–1321.

SMITH, J. D. & MCLEAN, S. R. 1977 Spatially averaged flow over a wavy surface. *J. Geophys. Res.* **82**, 1735–1746.

SNISHCHENKO, B. F. & KOPALIANI, Z. D. 1978 On the bedforms velocity in rivers and flumes. *Proc. State Hydr. Inst.* **252**, 30–37 (in Russian).

TSUJIMOTO, T. & NAKAGAWA, H. 1983 Sand wave formation due to irregular bed load motion. *Mechanics of Sediment Transport*, *Euromech. Colloq.* **156**, pp. 109–117.

https://doi.org/10.1017/S0022112097006708 Published online by Cambridge University Press